Synthesis and Characterization of Copolyimides Containing Fluorine and Silicon Surface Modifying Agents

John W. Connell[1], Christopher J. Wohl[1], Allison M. Crow[2], William T. Kim[2], Michelle H. Shanahan[3], Jereme R. Doss[3] and Yi Lin[3]*

[1]NASA Langley Research Center, Hampton, VA 23681, USA

[2]NASA Langley Research Summer Scholars, NASA Langley Research Center, Hampton, VA 23681, USA

[3]National Institute of Aerospace, 100 Exploration Way, Hampton, VA 23666, USA

ABSTRACT

Understanding the effects that monomer chemistries have on material properties allows for fine tuning of polymer synthesis for current and future applications. In order to develop polymeric based coatings that have minimal surface adhesion characteristics when exposed to a variety of contaminants, a more thorough understanding of fundamental structure-property relationships is needed. In the aeronautics field, one concept to improve fuel efficiency of future aircraft is to modify the wing design to enable laminar flow. There is a concern that contaminants such as insect residue and other debris will adhere to airflow surfaces and have sufficient height to disrupt laminar flow thereby increasing drag with concomitant loss of fuel efficiency. One potential solution would be a polymer surface or coating that prevents or minimizes adhesion of such contaminants. As part of a structure-property relationship study involving modification of surface properties, a series of copolyimides containing both fluorine and silicon surface modifying agents (SMAs) were prepared and characterized. Based on knowledge of structure-property relationships with polyimides containing either type of SMA, it was hypothesized that the combination of two different surface-modifying agents may lead to unique surface properties as the two SMAs competed for surface area at the polymer-air interface. Copolyimides for this study were prepared through a multi-step synthesis using an aromatic dianhydride with equimolar amounts of diamino functionalities comprised of an aromatic diamine along with two SMAs. Films were cast from copoly(amide acid) solutions that were subsequently thermally imidized under a nitrogen atmosphere. Polyimide films and coatings were characterized using differential scanning calorimetry (DSC), Fourier transform infrared spectroscopy (FTIR), ultraviolet–visible spectroscopy (UV-Vis), contact angle goniometry (CAG), scanning electron microscopy (SEM), and energy-dispersive X-ray spectroscopy (EDS) to determine chemical, thermal, and surface properties. Select samples were subject to high

velocity insect impacts in a small scale wind tunnel and the resulting residues were characterized for height and surface area and compared to those of a control surface.

KEYWORDS: Surface migration, coatings, laminar flow, insect impact tests, insect residue adhesion

INTRODUCTION

Over the past decade, a significant amount of work has gone into engineering surfaces to achieve significant improvements in adhesion and abhesion (i.e., anti-adhesion). A variety of approaches have been investigated that involve both chemical and topographical modifications to achieve desired surface characteristics and behavior for specific applications. One chemical approach has involved the use of surface modifying agents (SMAs) that contain fluorine or silicon atoms that are thermodynamically drawn to the low surface energy interface (i.e., often the air side of a solid-supported film) of a polymeric coating. Typically, the SMA has reactive functional groups such that it becomes covalently bound to the polymer backbone, chain end or in a pendant configuration. This approach has been demonstrated with many polymer families such as esters[1], urethanes[2-4], acrylates[5], siloxanes[6], and imides[7,8]. Thus, the approach of using silicon or fluorine containing SMAs is applicable to many different polymer types such that if it is effective with one, it will likely work with many others. By using skillful synthetic designs, other functional groups that normally would not be thermodynamically drawn to the surface can be placed adjacent to the fluorine or silicon atoms in the SMA and effectively transported there[9]. An added benefit of this approach is that the amount of SMA required to impart significant changes in surface properties is generally low, often less than 1% by weight, thus the bulk properties of the base polymer are minimally affected.

As a continuation of our efforts to engineer surfaces of materials that exhibit abhesive interactions for a variety of future NASA missions[7,8,10], copoly(imide alkyl ethers)s containing both pendant fluoro groups and siloxane backbone units were synthesized and characterized. This approach was designed to investigate the effects of combining the inherent properties of the copolymer components, namely the

high thermal stability, mechanical strength, and radiation resistance of polyimides[11], and the surface migrating characteristics of both the oxetane-derived alkyl ethers that contain pendant fluoro groups, and the siloxane containing backbone segments. It was hypothesized that the combination of these material properties could provide a mechanically robust coating while minimizing surface adhesion of species such as ice and insect residue on future aircraft, and Lunar or Martian dust on future exploration missions[7]. For example, NASA recently conducted research under the environmentally responsible aviation (ERA) program to reduce fuel consumption and engine emissions[12]. One approach which has shown potential to reduce fuel consumption is to utilize laminar flow more extensively across wing surfaces in future aircraft designs. Contamination by particles and debris such as insect residue can potentially disrupt laminar flow depending upon the flight conditions and the location and height of the debris, and consequently increase drag[13,14]. One potential method to mitigate adhesion of undesirable species to airflow surfaces is to use a coating which minimizes adhesion and/or allows for facile cleaning. In this work, the synthesis, characterization, and bench-top wind tunnel-based insect impact tests results are described. The surface migration behavior of the Si and F containing SMAs in the copolymers was investigated using contact angle goniometry (CAG) and energy-dispersive X-ray spectroscopy (EDS). The results of this study are presented herein.

EXPERIMENTAL

Materials and Methods.

The amino-terminated alkyl ether containing pendant fluorinated groups (AEFO) was derived from the commercially available hydroxyl-terminated alkyl ether oligomer (PF7002, Omnova, molecular weight 1971 g/mole) following a previously described method[8]. The aminopropyl-terminated siloxane oligomer (DMS-A11, Gelest, molecular weight 1150 g/mole) was used as received. 3,3',4,4'-biphenyltetracarboxylic dianhydride (s-BPDA, ChrisKev Company Inc., T_m = 292 °C) was purified by refluxing in a 3:1 ratio of acetic acid:acetic anhydride, and isolated by filtration and vacuum drying at 120 °C for 6 h. 2,2-bis(3,4-dicarboxyphenyl)hexafluoropropane dianhydride (6FDA, Clariant Corporation,

T_m = 242 °C) was vacuum dried prior to use. 1,3-bis(3-aminophenoxy)benzene (1,3-APB, T_m = 107-108 °C) was used as received from Kriskev Inc. All other reactants and solvents were used as received from commercial vendors. Inherent viscosities (η_{inh}) were determined at 25 °C on the copoly(amide acid) solutions using an Ubelohde viscometer and solution concentration of 0.5 g dL^{-1}. Proton nuclear magnetic resonance (^{1}H NMR) spectra were used to calculate molecular weight of the AEFO oligomers and were recorded on a Bruker (Avance 300) Multinuclear NMR Spectrometer operating at 300.152 MHz. All spectra were collected in $CDCl_3$ and the determined chemical shifts were relative to tetramethylsilane (TMS) at δ = 0 PPM. Differential scanning calorimetry (DSC) was conducted using a Setaram Instrumentation DSC 131 with a heating rate of 15 °C/min over a temperature range of 30 to 300 °C. Contact angle goniometry (CAG) data were collected using a First Ten Ångstroms FTA 1000B contact angle goniometer. Sessile and tilting axis contact angles were measured for each sample using an 8 µL drop for water and ethylene glycol, and a 2.5 µL drop for methylene iodide. Attenuated total reflectance infrared (ATR-IR) spectroscopy was conducted with a Thermo-Nicolet FT-IR 300 spectrometer equipped with a Thunderdome Swap-Top single reflection ATR module to confirm imidization of the copolyimides after thermal cure. A Mitutoyo Corp Absolute LCD Digimatic micrometer was used to measure film thicknesses. Optical absorption spectra were obtained using a Perkin-Elmer Lambda 900 ultraviolet visible/near infrared (UV Vis/NIR) spectrometer. Energy-dispersive X-ray spectroscopy (EDS) studies were conducted using a Thermo Scientific Noran System 7 X-Ray microanalysis system attached to a Hitachi S-5200 field emission scanning electron microscope (SEM). Samples were sputtered with a thin layer (~3 nm) of Au/Pd prior to analysis. The acceleration voltage during the analysis was 20 kV. The EDS spectral acquirement was conducted at a time constant of 71,400 counts per second (cps). The EDS mapping was acquired at 30 frames at 10 s/frame with a time constant of 227,000 cps.

Synthesis of Polymers.

The following is a general procedure used to prepare the homo and copolyimides used in this study. Poly(amide acid)s were prepared by the addition reaction of either s-BPDA or 6FDA and 1,3-APB and

the desired molar quantities of AEFO and DMS-A11 in N,N-dimethylacetamide (DMAc) at a 20-25% solids content at room temperature under nitrogen. To prevent excessive solution viscosity build-up, a stoichiometric ratio of diamines to dianhydride of 0.85 to 1.0 was used for the synthesis of the homopolymers whereas the copolymers were prepared at a 1.0 to 1.0 stoichiometric ratio. Inherent viscosities of the poly(amide acid)s were measured on 0.5% (wt/wt) solutions in DMAc at 25 °C using an Ublehold viscometer. Films were subsequently cast from the poly(amide acid) solutions on stainless steel plates using a doctor blade and placed in a forced air-drying chamber until tack-free. Films were then thermally imidized under nitrogen using a cure cycle with stages at 150, 175, 200, and 250 °C, with at least a 40 min hold at each temperature. Complete imidization under these conditions was confirmed by ATR-FTIR (data not shown). The films were subsequently removed from the stainless steel plates by immersion in water and used to perform the various characterizations and tests described herein.

Insect Impact Testing.

To emulate flight conditions under which insect impact events occur, controlled flightless fruit fly (*drosophila melanogaster*) impact studies were conducted inside a benchtop wind tunnel. An insect delivery device was utilized to propel the fruit fly at velocities representative of aircraft takeoff speeds[15]. Testing was conducted using a custom-built pneumatic insect delivery device constructed from a VACCON HIGHVAC HVP series 300-Venturi vacuum pump that was modified with an extended delivery nozzle to enable accurate positioning of the insect impact site. Testing was conducted at ambient temperature (approximately 25°C) and about 50-60% relative humidity. For each event, the airflow was turned on prior to feeding a single insect into the insertion port. The suction force rapidly propelled the insect from the delivery port for impact on the test surface. High-speed photography was obtained during impact events using a Vision Research Phantom 12 camera at a frame rate of 50,000 frames per second.

Velocity measurements were obtained from high-speed photography of the insect trajectory against a 6 cm grid with 0.5 cm graduations. The air pressure was approximately 0.12 MPa. Insect velocities were

determined by dividing the distance by the time, determined from the frame count, required for the insect to traverse the set distance. The velocities were determined to be 234 ± 29 kph; well above that requisite for rupture of a fruit fly exoskeleton which is approximately 50 kph.

The heights of remaining insect residue were characterized using a FRT of America optical surface profilometer (Microprof 100). Data were collected over the entire region containing visible insect residues at a resolution of 5 μm between data points and 40 μm line to line. Several processing steps were performed on the collected topographical data including: segmentation to remove false zero readings, fitting the baseline to a second-order polynomial, and masking any edge and surface defects. Areal coverage was determined using grain analysis that identified and summed all features above the lowest permissible data plane, typically 8-15 μm, as individual grains. The data plane threshold above the established baseline was necessary to sufficiently separate insect residue features from substrate anomalies.

RESULTS AND DISCUSSION

Polymer and Copolymer Synthesis.

Homopolyimide films of the respective dianhydride and 1,3-APB were prepared following the procedure described in the experimental section. These served as controls in order to make comparisons with the surface properties of the corresponding copolymers containing fluorine and silicon SMAs. The copolymers were prepared as shown in Figure 1. Note that this synthetic approach yields random copolymers. The copoly(amide acid) solutions were generally an opaque yellow color.

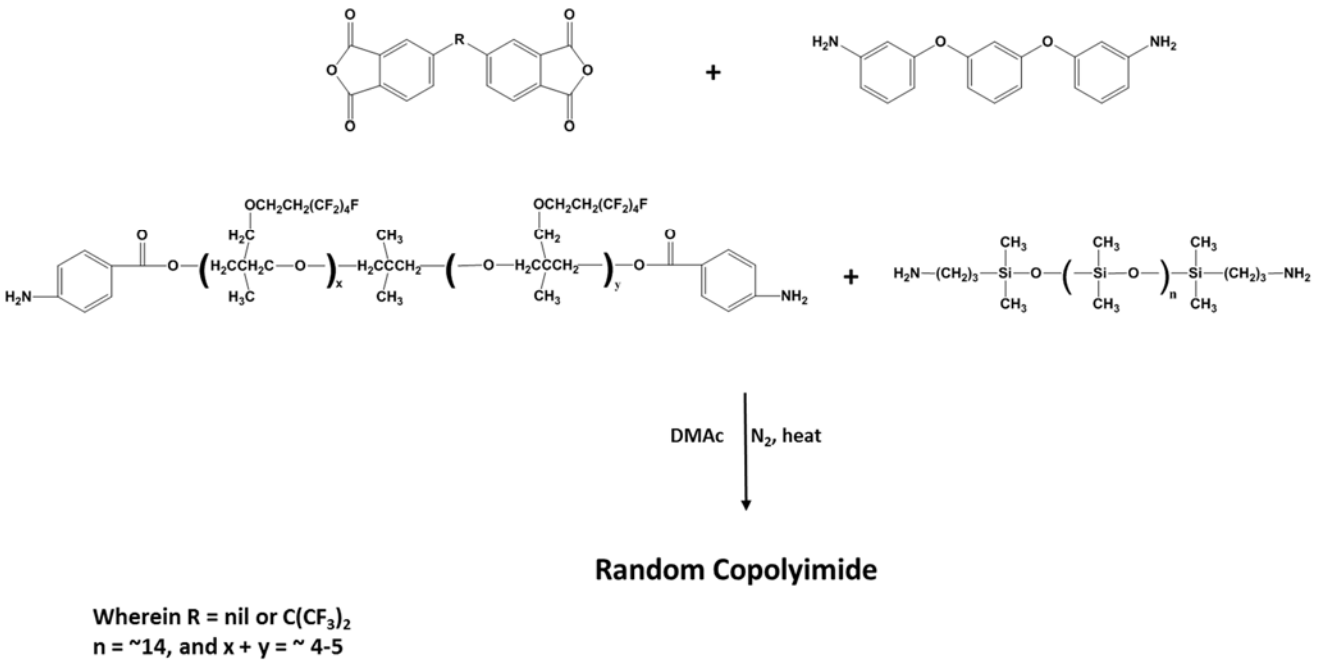

Figure 1. Schematic for the preparation of the random copolyimides

The poly(amide acid) solutions were doctored onto stainless steel plates and dried to a tack-free state under flowing dry air. Stainless steel plates were used instead of glass to make removal of the films easier, as the copolymers bonded tenaciously to glass. The cast films on stainless steel plates were subsequently placed in a nitrogen oven and stage heated to 150, 175, 200, and 250 °C, with at least a 40 min hold at each temperature. The use of the nitrogen atmosphere and lower final cure temperature than is typically used for thermal imidization was necessary to prevent thermal oxidation of the aliphatic species in the SMAs. Complete imidization under these conditions was confirmed by ATR-FTIR. The adsorption band observed in the spectra of the amide acid films at 1547 cm^{-1} was absent from the spectra of the corresponding films after thermal treatment (data not shown). Adsorption bands assigned to imide functionalities were observed at 1721 and 1784 cm^{-1} after thermal treatment. After thermal imidization, the films were yellow and opaque in appearance indicating some degree of phase segregation. The air side of the films had a higher gloss and felt more slippery to the touch than the steel plate side of the films. The composition and preliminary characterization of the 6FDA and BPDA containing copolymers prepared in this study are presented in Tables 1 and 2, respectively.

Table 1. Composition and Characterization of 6FDA Containing Polymers and Copolymers

Designation	Stoichiometric Composition, Mole%	η_{inh}, dL/g	T_g, °C
6FDA Control	6FDA and APB	0.43	204
6FDA-1	5% AEFO, 5% DMS	0.31	185
6FDA-2	1% AEFO, 1% DMS	0.18	197
6FDA-3	3% AEFO, 3% DMS	0.25	190
6FDA-4	5% AEFO, 1% DMS	0.25	190
6FDA-5	1% AEFO, 5% DMS	0.29	189
6FDA-6	5% AEFO, 3% DMS	0.20	191
6FDA-7	3% AEFO, 5% DMS	0.32	186
6FDA-8	0.5% AEFO, 0.5% DMS	0.24	201
6FDA-9	3% AEFO, 1% DMS	0.31	189
6FDA-10	1% AEFO, 3% DMS	0.19	191

Table 2. Composition and Characterization of BPDA Containing Polymers and Copolymers

Designation	Stoichiometric Composition, Mole%	η_{inh}, dL/g	T_g, °C
BPDA Control	BPDA and APB	0.26	205
BPDA-1	5% AEFO, 5% DMS	0.32	193
BPDA-2	1% AEFO, 1% DMS	0.25	198
BPDA-3	3% AEFO, 3% DMS	0.27	196
BPDA-4	5% AEFO, 1% DMS	0.19	197
BPDA-5	1% AEFO, 5% DMS	0.33	189
BPDA-6	5% AEFO, 3% DMS	0.40	196

BPDA-7	3% AEFO, 5% DMS	0.44	194
BPDA-8	0.5% AEFO, 0.5% DMS	0.33	203
BPDA-9	3% AEFO, 1% DMS	0.30	202
BPDA-10	1% AEFO, 3% DMS	0.26	200

As can be seen in Tables 1 and 2, the inherent viscosities were generally around 0.30 dL/g for the copolymers. All of the copolymers formed films that were tough, flexible, and opaque. The glass transition temperatures (T_gs) decreased with increasing SMA content as expected since they are significantly more flexible than the aromatic imide segments.

Surface Characterization of Copolymer Films.

CAG was utilized to characterize the surface properties of the copolymers. Contact angle measurements were collected using water, ethylene glycol and diiodomethane on both the air and steel plate sides of the copolymer films and used to calculate the surface energy which is presented in Tables 3 and 4.

Table 3. Surface Characterization of 6FDA Copolyimides

Designation	Stoichiometric Composition, Mole%	Advancing Water Contact Angle, θ		Surface Energy, mJ/m^2	
		Air Side	Plate Side	Air Side	Plate Side
6FDA Control	6FDA and APB	94	97	24.3	21.7
6FDA-1	5% AEFO, 5% DMS	108	102	13.5	15.9
6FDA-2	1% AEFO, 1% DMS	106	105	21.1	13.9
6FDA-3	3% AEFO, 3% DMS	106	106	17.8	12.1
6FDA-4	5% AEFO, 1% DMS	106	111	19.8	13.4
6FDA-5	1% AEFO, 5% DMS	98	105	20.0	12.6
6FDA-6	5% AEFO, 3% DMS	104	112	22.3	14.5

6FDA-7	3% AEFO, 5% DMS	106	103	17.8	13.7
6FDA-8	0.5% AEFO, 0.5% DMS	99	92	23.6	23.9
6FDA-9	3% AEFO, 1% DMS	105	112	21.2	14.4
6FDA-10	1% AEFO, 3% DMS	104	107	22.2	17.6

Table 4. Surface Characterization of BPDA Copolyimides

Designation	Stoichiometric Composition, Mole%	Advancing Water Contact Angle, θ		Surface Energy, mJ/m^2	
		Air Side	Plate Side	Air Side	Plate Side
BPDA Control	BPDA and APB	89	90	22.7	20.5
BPDA-1	5% AEFO, 5% DMS	114	108	14.1	12.4
BPDA-2	1% AEFO, 1% DMS	103	92	13.5	18.7
BPDA-3	3% AEFO, 3% DMS	108	98	14.6	16.0
BPDA-4	5% AEFO, 1% DMS	106	94	20.8	17.6
BPDA-5	1% AEFO, 5% DMS	108	102	14.1	14.5
BPDA-6	5% AEFO, 3% DMS	93	120	17.3	10.7
BPDA-7	3% AEFO, 5% DMS	109	112	15.8	11.4
BPDA-8	0.5% AEFO, 0.5% DMS	105	117	18.2	12.0
BPDA-9	3% AEFO, 1% DMS	103	109	15.1	12.3
BPDA-10	1% AEFO, 3% DMS	100	94	17.1	19.6

The water contact angles for all of the copolymers were higher than those of the control. Likewise, the surface energies were lower for the copolyimide films than the control. The advancing and receding contact angles were also measured on both sides of the film samples by tilting the machine axis to 60° after measuring the sessile drop contact angle. In nearly all cases for the 6FDA samples, the steel plate

side of the films exhibited lower surface energies than the air side. This observation correlates with the fluorine concentration being slightly higher on the steel plate side (see EDS section). For the BPDA containing films, most exhibited lower surface energies on the steel plate side as well. These results indicate that the SMAs are affecting the surface properties on both sides of the films, but generally to a more significant degree on the steel plate side.

UV-VIS Spectroscopy.

The addition of SMAs altered the visual appearance of the copolyimide films. The homopolyimide control film was transparent while those containing the SMAs were translucent and yellow to off-white in color. The dependence of this translucency and color increase on increasing SMA concentration suggested that the SMAs could be forming micelle-like structures within the polyimide bulk, similar to what has been seen at high SMA concentrations in other systems[16]. UV-Vis spectroscopy was conducted on thin films and the % transmittance at 500 nm was analyzed (Figure 2). A full spectrum was also run for representative samples of copolyimides with both high and low concentrations of SMAs (data not shown). The data confirmed that the homopolyimide has very high % transmittance values and the copolyimides with 0.5% equal molar concentration of both SMAs (6FDA-8 and BPDA-8) have only slightly lower values, consistent with visual observations. The 3% and 5% equal molar SMA concentrations showed significantly lower % transmittance values. Analysis of thickness-dependent % transmittance at 500 nm showed a decrease in % transmittance upon increased AEFO content. The data, excluding films with greater DMS than AEFO content, were fitted to a single exponential decay function. The decay rate, Γ, was used to calculate an approximate SMA domain size, *D*, assuming that the reduction in % transmittance at 500 nm could be fully attributed to scattering. This was achieved by utilizing the equation for determination of particle size from dynamic light scattering:

$$\Gamma = q^2 D \qquad (1)$$

where *q* is:

$$q = \frac{4\pi n_o}{\lambda} \sin\left(\frac{\theta}{2}\right) \quad (2)$$

Using values for the refractive index, n_o, and the detection angle, θ, of 1.6[17] and π (180°), respectively, as well as a λ value of 500 nm, D was calculated to be approximately 400 nm. As will be shown below, this agrees with the SMA-enriched domains observed using EDS. Similar analysis of the films with equal or greater DMS content (data not shown) showed no correlation providing further support that the fluorine containing SMA influenced the absorbance at 500 nm.

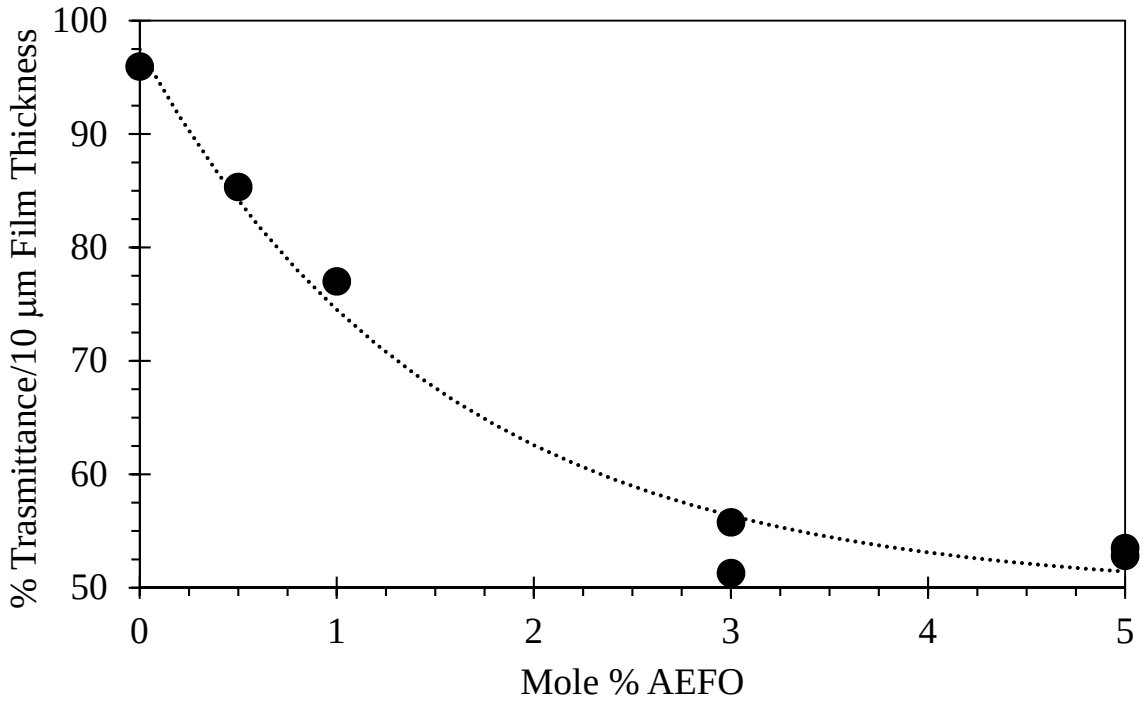

Figure 2. Film thickness dependent % transmittance at 500 nm versus AEFO content. The data shown here are for a nominal film thickness of 10 μm as determined by calculating the % transmittance value for a film thickness of 1 μm.

Energy-Dispersive X-Ray Spectroscopy.

Select samples were investigated using SEM/EDS in order to determine the surface fluorine and silicone content as well as the presence of phase segregation. EDS elemental data were quantified but not calibrated against any known standards. All experiments were carried out under exactly the same conditions, thus the relative changes can be viewed as semi-quantitative. Analyses were conducted on both the air side and steel plate side of the film samples. The surface elemental analysis as measured by EDS for select films are presented in Table 5. For the 6FDA based samples, the fluorine content was considerably higher than theoretical and evenly distributed on both sides of the film surfaces. The silicon distribution was also higher than theoretical with comparable amounts on both the air and steel side surfaces. In contrast, the BPDA based samples had much less fluorine and more variability in concentration on the air and steel plate side surfaces. Also, the silicon concentration was generally higher compared to the 6FDA samples, and exhibited more variability between the air side and steel plate side. In looking at the weight ratios of the fluorine:oxygen (F:O) and silicon:oxygen (Si:O) it can be observed that in most cases the ratios were higher than the theoretical indicating surface enrichment.

Table 5. EDS Characterization of Copolyimides

Sample (%AEFO and %DMS)	Film Orientation	Weight Percentage (%)					Weight Ratio	
		C	N	O	F	Si	F:O	Si:O
6FDA Control	Air	35.8	8.8	22.8	32.4	0.3	1.42	0.01
	Steel plate	36.2	8.5	22.7	32.3	0.4	1.42	0.02
	Theory	*65.1*	*4.1*	*14.1*	*16.7*	*0*	*1.18*	*0*
6FDA-4 (5%, 1%)	Air	35.2	7.0	20.5	35.9	1.4	1.75	0.07
	Steel plate	35.2	7.1	21	35.1	1.6	1.67	0.08
	Theory	*61.9*	*3.6*	*13.9*	*20.1*	*0.5*	*1.45*	*0.04*
6FDA-8 (0.5%, 0.5%)	Air	36.7	8.4	21.7	32.4	0.8	1.49	0.04
	Steel plate	36.5	8.5	22.0	32.1	0.9	1.46	0.04
	Theory	*64.6*	*4*	*14.1*	*17*	*0.3*	*1.21*	*0.02*
6FDA-10 (1%, 3%)	Air	35.8	7.8	20.7	30.6	5.1	1.48	0.25
	Steel plate	36.7	7.9	21.0	30.4	4.1	1.45	0.20

	Theory	*63.4*	*4*	*14.3*	*16.8*	*1.6*	*1.17*	*0.11*
BPDA Control	Air	49.5	14.2	35.7	0.4	0.2	0.01	<0.01
	Steel plate	47.5	13.4	37.4	1.4	0.3	0.04	0.01
	Theory	*76.7*	*5.3*	*18*	*0*	*0*	*0*	*0*
BPDA-4 (5%, 1%)	Air	45.6	12.9	31.1	8.3	2.1	0.27	0.07
	Steel plate	37.9	7.7	25.1	26.8	2.4	1.07	0.10
	Theory	*71.1*	*4.5*	*17.2*	*6.6*	*0.6*	*0.38*	*0.03*
BPDA-8 (0.5%, 0.5%)	Air	46.5	14.1	34.7	2.9	1.8	0.08	0.05
	Steel plate	45.9	13.4	31.3	7.8	1.7	0.25	0.05
	Theory	*75.8*	*5.1*	*18*	*0.8*	*0.4*	*0.04*	*0.02*
BPDA-10 (1%, 3%)	Air	48.2	11.6	31.2	3.8	5.2	0.12	0.17
	Steel plate	48.4	11.3	30.4	3.8	5.0	0.13	0.17
	Theory	*73.6*	*4.9*	*18.1*	*1.4*	*2.1*	*0.08*	*0.12*

Elemental mapping experiments were conducted to further probe the sample morphology with representative samples shown in Figures 3-6. In general, samples that contained low DMS (i.e. silicon) content relative to the AEFO (i.e. fluorine) content exhibited uniform silicon distribution (i.e., 6FDA-2, 4, and 9, BPDA-2, 4, and 9, data not shown). Samples with higher AEFO content generally exhibited uniform distribution of Si (Figure 3). Interestingly, in comparing 6FDA-6 (Figure 3) with BPDA-6 (Figure 4), the only compositional difference being the dianhydride used, some phase segregation of the fluorine was observed (Figure 4). Samples with equivalent or higher content of DMS compared to the AEFO exhibited some degree of phase segregation with both fluorine and silicon enriched domains appearing on the air side predominately (i.e., 6FDA-3, 5 and BPDA-3, 5), and sometimes on both surfaces (6FDA-7 and BPDA-7, Figures 5 and 6, respectively).

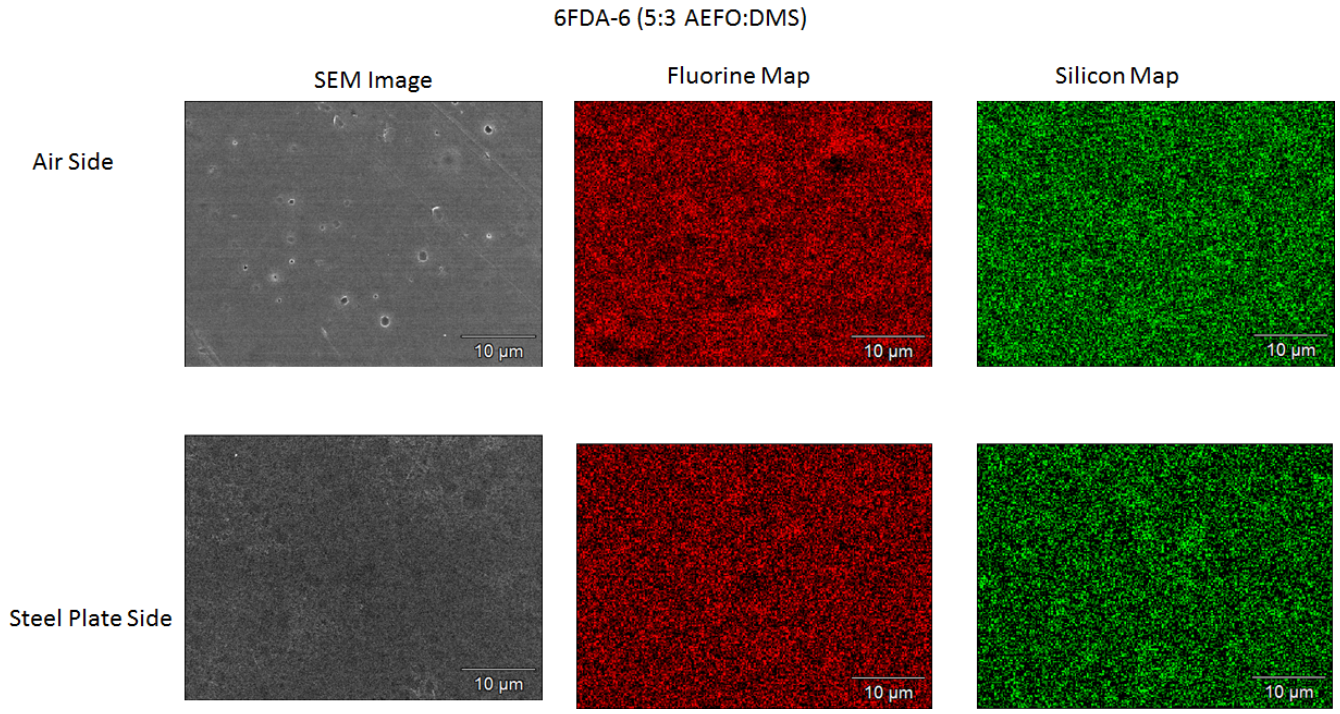

Figure 3. Elemental map of 6FDA-6 showing even distribution of F and Si on both surfaces.

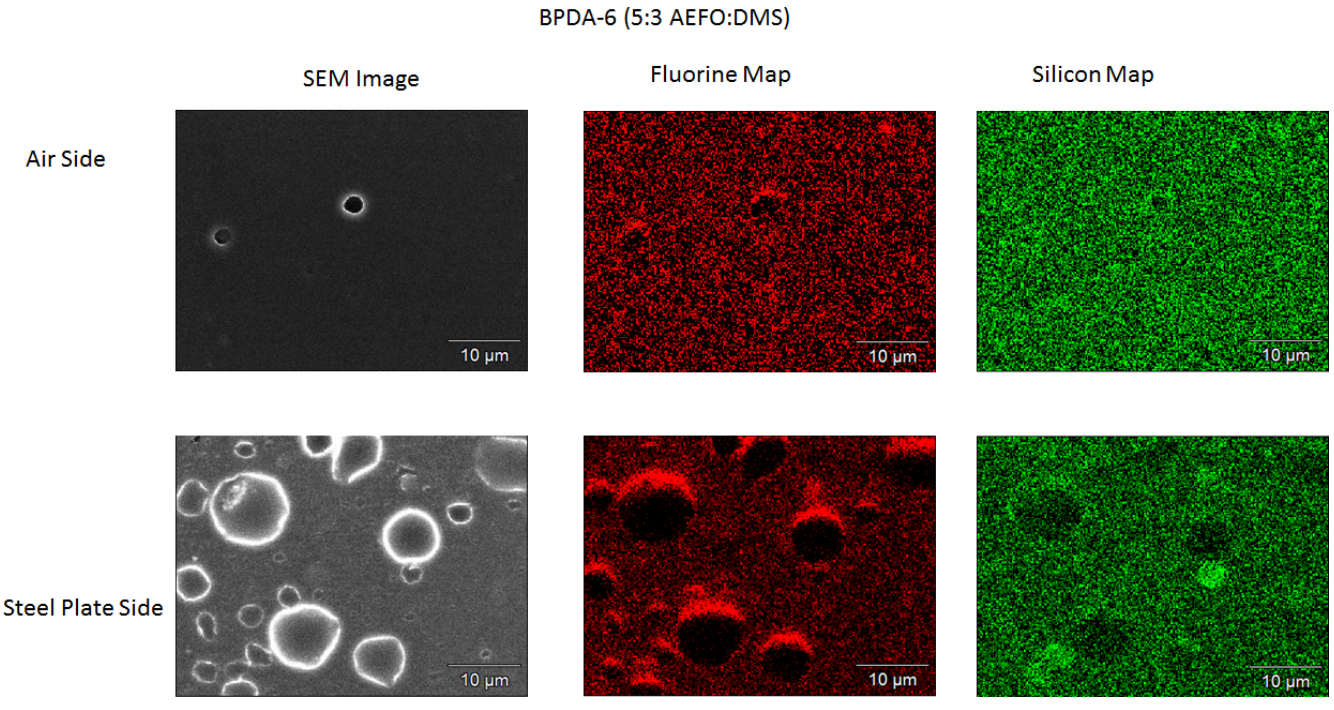

Figure 4. Elemental map of BPDA-6 showing fluorine enriched phases.

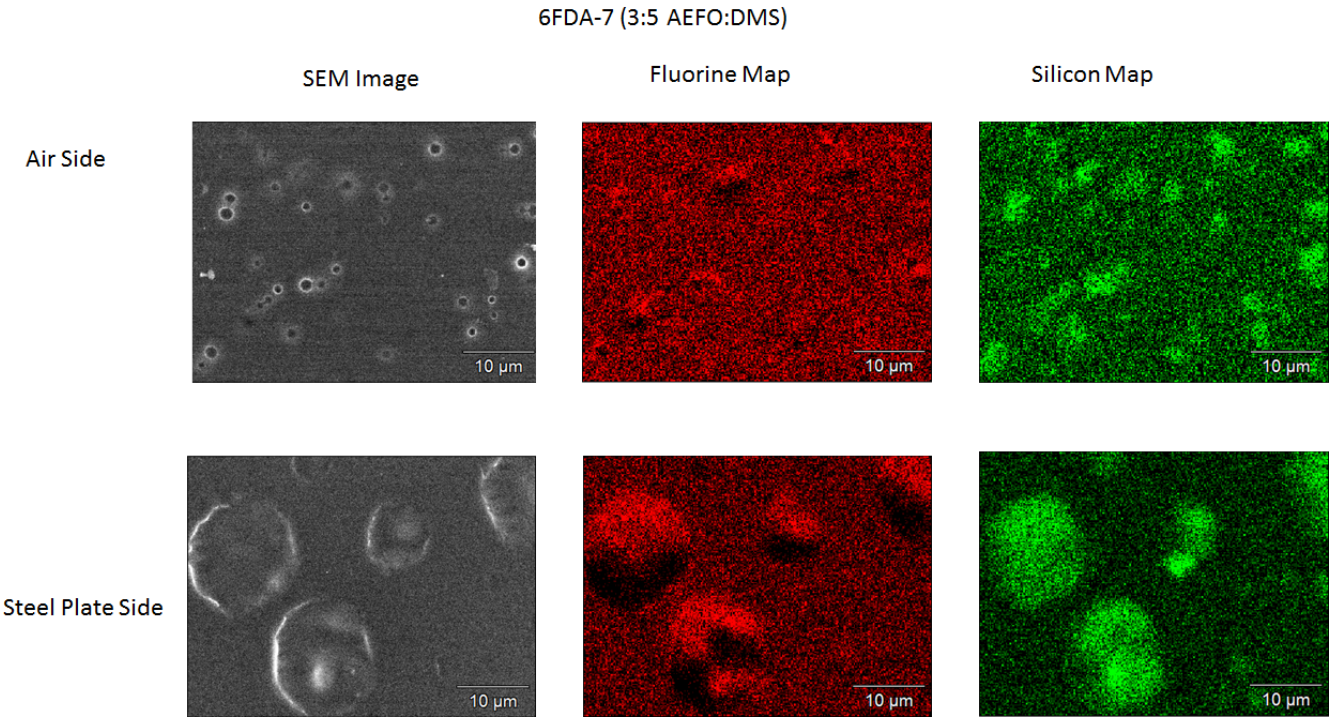

Figure 5. Elemental map of 6FDA-7 showing silicon enriched phases on both surfaces.

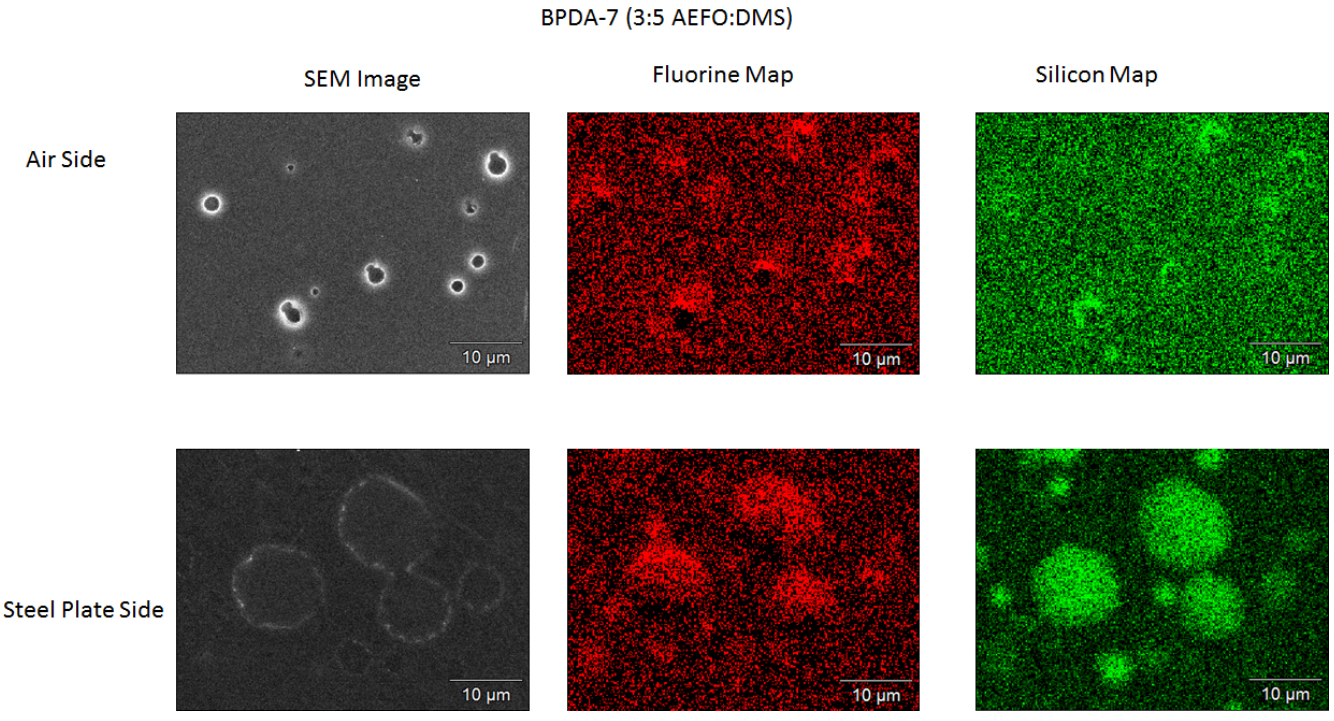

Figure 6. Elemental map of BPDA-7 showing silicon enriched phases on both surfaces.

Insect Impact Tests.

Select samples were subjected to insect impact tests in a small scale wind tunnel. The film samples were mounted to a flat aluminum plate and impacted with flightless fruit flies under the conditions described in the experimental section. The impacts were recorded using high speed video to ensure the fruit flies were whole prior to impact and to help visualize the impact and subsequent release processes. At least 3 impacts per sample were recorded and the remaining residues were subsequently characterized for height and aerial coverage using optical profilometry. Polyimide films (6FDA control and BPDA control) comprised of the same monomers, but without any DMS or AEFO were used as the respective controls to compare the insect impact residue heights and surface areal coverage.

Residue Heights and Areal Coverage

The residue heights and areal coverage of remaining insect residue after impact for all the samples tested are presented in Figures 7 and 8, respectively. Nearly all of the data were collected using the air side of the film, however in two cases, the steel plate side was tested (BPDA-1 and BPDA-8). In most cases, the residue heights and areal coverages for the copolyimide coatings were less than those of the controls with the main exception being both 6FDA-5 and BPDA-5 (both contain 1% DMS and 5% AEFO). Also, in most cases there was not a great difference in the heights of the 6FDA versus BPDA copolyimides in which they contained the same relative amounts of the SMAs. The exceptions being BPDA-4 and BPDA-10 which exhibited a much lower residue height than the control and the corresponding 6FDA samples.

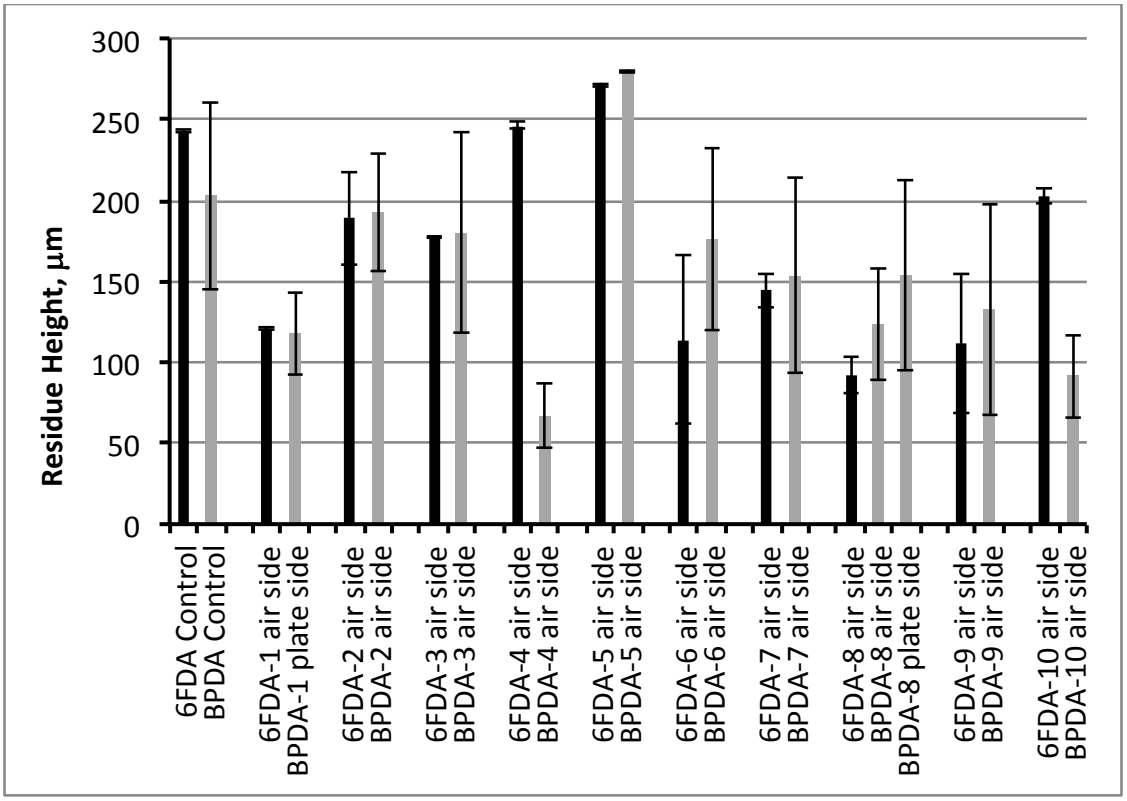

Figure 7. Residual insect residue height remaining after impact.

Residue Areal Coverage

The 6FDA samples exhibited more areal coverage than the corresponding BPDA samples in most cases. There did not seem to be any correlation between the samples that exhibited phase segregation by EDS and height or areal coverage. In comparing the one sample which had both the air side and the steel plate side of the sample tested, the air side exhibited a lower areal coverage.

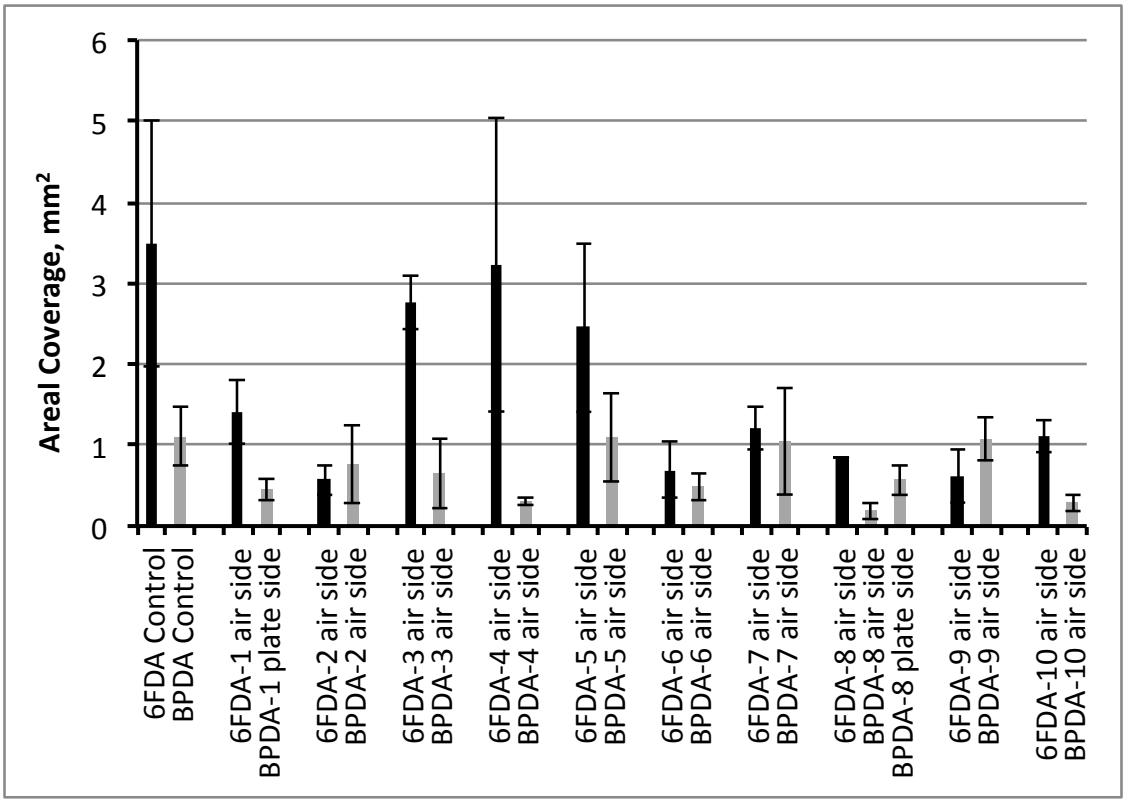

Figure 8. Residual insect residue areal coverage remaining after impact.

As a means to further analyze these test results, as they relate to the overall performance of these materials towards mitigating insect residue adhesion, the residual height was plotted against the residual areal coverage and is presented in Figure 9. The best performers appear in lower left-hand corner of this chart and are clearly the BPDA based samples (light colored diamonds). Most of the copolyimides exhibited a reduction in both insect residue height and areal coverage compared to their respective controls, with the best two performers being BPDA based (BPDA-4 and -10). Interestingly, the corresponding 6FDA copolymers which contained the same amounts of SMAs (6FDA-4 and -10) did not perform nearly as well. These results suggest that samples with high fluorine content are less effective at mitigating insect adhesion. For lower fluorine content samples where fluorine is only provided by SMAs, there was no clear dependence of insect residue mitigation on the fluorine content. However, the two best performers did contain medium amount of silicon-containing SMA (1% and 3% DMS) that is enriched on the surfaces. It is interesting that higher content ones (5% DMS, BPDA-1, -5 and -7) did not perform as well,

possibly due to more phase segregation as seen in the EDS results. With overwhelming presence of fluorine in the cases of 6FDA samples, the effect of silicon-containing SMAs became diminished.

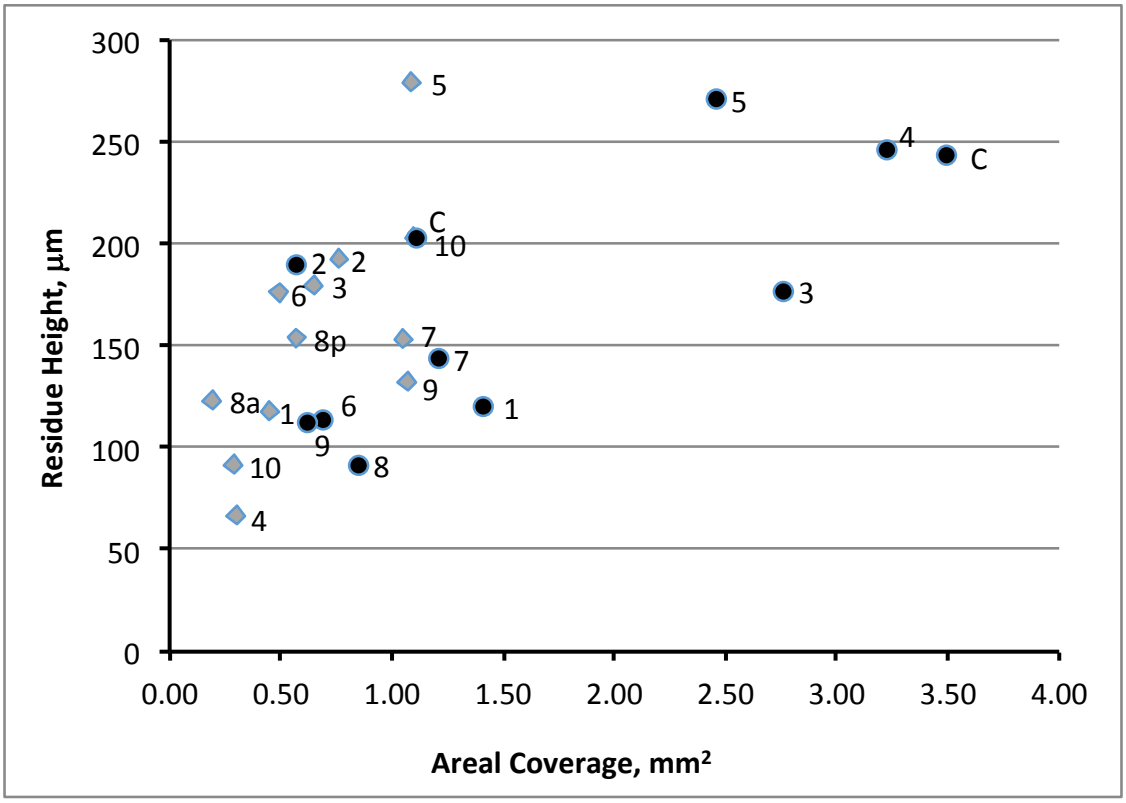

Figure 9. Plot of areal coverage versus height of insect residue. Dark circles are 6FDA based copolymers and diamonds are BPDA based copolymers. C corresponds to the respective control, and the numbers correlate with those in sample designation numbers in Tables 1 and 2.

SUMMARY

A series of copolyimides containing both silicon and fluorine surface modifying agents were prepared and characterized. Based on contact angles measurements, surface energy calculations and energy dispersive spectroscopy, the surface modifying agents migrated to a comparable extent to both the air surface and the stainless steel substrate surface of copolyimide coatings. Phase segregation was observed visually by the opacity of films, and confirmed by EDS analyses. Results of small scale wind tunnel insect

impact tests indicated that the BPDA based copolyimides provided better performance in terms of residual insect residue height and areal coverage. The current results suggest that a moderate amount of silicon-containing SMA can be beneficial to insect residue mitigation, while large amount of fluorine on the polyimide surface led to increased insect residue adhesion.

ACKNOWLEDGMENTS

Mr. Joseph Dennie (NASA Intern Fellowship Program) for conducting some of the contact angle goniometry measurements. Mr. Paul Bagby (NASA) for high speed video recording and analyses. Dr. Joseph G. Smith, Jr. for technical discussions.

AUTHOR INFORMATION

Corresponding Author

*E-mail: john.w.connell@nasa.gov. Phone: (757) 864-4264.

REFERENCES

1. Xiong, J.; Xia, L.; Shentu, B.; Weng, Z., Synthesis of Fluoroalkyl-Modified Polyester and its Application in Improving the Hydrophobicity and Oleophobicity of Cured Polyester Coatings. *J. Appl. Polym. Sci.* **2014,** *131* (2), 39812.

2. Khayet, M.; Suk, D. E.; Narbaitz, R. M.; Santerre, J. P.; Matsuura, T., Study on Surface Modification by Surface-Modifying Macromolecules and its Applications in Membrane-Separation Processes. *J. Appl. Polym. Sci.* **2003,** *89* (11), 2902-2916.

3. Tang, Y. W.; Santerre, J. P.; Labow, R. S.; Taylor, D. G., Synthesis of Surface-Modifying Macromolecules for Use in Segmented Polyurethanes. *J. Appl. Polym. Sci.* **1996,** *62* (8), 1133-1145.

4. Rahman, M. M.; Lee, I.; Chun, H.-H.; Kim, H. D.; Park, H., Properties of Waterborne Polyurethane-Fluorinated Marine Coatings: The Effect of Different Types of Diisocyanates and Tetrafluorobutanediol Chain Extender Content. *J. Appl. Polym. Sci.* **2014,** *131* (4), 39905.

5. An, Q.; Xu, W.; Hao, L.; Huang, L., Cationic Fluorinated Polyacrylate Core-Shell Latex with Pendant Long Chain Alkyl: Synthesis, Film Morphology, and its Performance on Cotton Substrates. *J. Appl. Polym. Sci.* **2013,** *127* (3), 1519-1526.

6. Zhang, W.; Zheng, Y.; Orsini, L.; Morelli, A.; Galli, G.; Chielleni, E.; Carpenter, E. E.; Wynne, K. J., More Fluorous Surface Modifyer Makes it less Oleophobic: Fluorinated Siloxane Copolymer/PDMS Coating. *Langmuir* **2010,** *26* (8), 5848-5855.

7. Wohl, C. J.; Atkins, B. M.; Belcher, M. A.; Connell, J. W., Synthesis, Characterization, Topographical Modification, And Surface Properties Of Copoly(Imide Siloxane)s. *High Perform. Polym.* **2012,** *24* (1), 40-49.

8. Wohl, C. J.; Foster, L. L; Applin, S. I.; Connell, J. W., Synthesis and Surface Characterization of Copoly(Imide Alkyl Ether)s Containing Pendant Fluoroalkyl Groups. *J. Appl. Polym. Sci.* **2015**, DOI: 10.1002/APP.41538.

9. Wynne, K.; Makal, U.; Kurt, P.; Gamble, L., Model Fluorous Polyurethane Surface Modifiers Having Co-polyoxetane Soft Blocks with Trifluoroethoxymethyl and Bromomethyl Side Chains. *Langmuir* **2007,** *23*, 10573 - 10580.

10. Wohl, C. J.; Belcher, M. A.; Ghose, S.; Connell, J. W., Modification Of The Surface Properties Of Polyimide Films Using POSS Deposition And Oxygen Plasma Exposure *Appl. Surf. Sci.* **2009,** *255* (18), 8135 - 8144.

11. *Polyimides*. Wilson, D.; Stenzenberger, H. D.; Hergenrother, P. M., Eds. Chapman and Hall: New York, 1990.

12. Collier Jr., F. S., Overview of ERA Technologies and N+2 Integrated Vehicle Concepts. In *AIAA 50th Aerospace Sciences Meeting*, Nashville, TN, United States of America, 2012.

13. Joslin, R., Aircraft Laminar Flow Control. *Ann. Rev. Fluid Mech.* **1998,** *30*, 1-29.

14. Young, T.; Humphreys, B., Liquid Anti-contamination Systems for Hybrid Laminar Control Flow Aircraft: A Review of Critical Issues and Important Experimental Results. *Proc. Instn. Mech. Engrs. G. J. Aerospace Eng.* **2004,** *218* (4), 267-277.

15. Siochi, E. J.; Wohl, C. J.; Smith, J. G., Jr.; Gardner, J. M.; Penner, R. K.; and Connell, J. W.: "Engineered Surfaces For Mitigation Of Insect Residue Adhesion", SAMPE Spring 2013 Electronic Conference Proceedings, May, 2013.

16. Zhang, Wei; Zheng, Ying; Orsini, Lorenzo; Morelli, Andrea; Galli, Giancarlo; Chiellini, Emo; Carpenter, Everett; and Wynne, Kenneth J., More Fluorous Surface Modifier Makes it Less Oleophobic: Fluorinated-Siloxane Copolymer/PDMS Coatings, Langmuir, 2010, 26 (8), 5848–5855.

17. Lee, Choonkeun; Seo, Jongchul; Shul, Yonggun; and Han, Haksoo, Optical Properties of Polyimide Films. Effect of Chemical Structure and Morphology. *Polymer Journal*, **2003**, 35 (7), 578-585.